Gams, M., Planinc, I., Saje, M. 2007. A heuristic viscosity-type dissipation for high frequency oscillation damping in time integration algorithms. *Computational mechanics* 41,1: 17-29 DOI: 10.1007/s00466-007-0165-y.

Computational Mechanics manuscript No.
(will be inserted by the editor)

Gams M. · Planinc I. · Saje M.

A heuristically enhanced viscosity type damping for damping high frequency oscillations in time-step integration algorithms

Received: date / Accepted: date

Abstract A viscosity type damping on strains is enhanced using a heuristic approach for introducing a controllable high frequencies numerical dissipation into one-step time integration scheme. The basic idea of the approach is to apply damping at places, where it is needed, at times when it is needed. To this end a computationally efficient algorithm for identifying the need for damping is developed. The identifying algorithm keeps track of a user prescribed number of recent changes of signs of strains increments, which enables it to decide whether damping should be engaged or not. A special scaling function for damping is introduced to smoothen the transition between damped and undamped phases. The approach is verified in the geometrically exact plane beam dynamics, but is in principle entirely general.

Keywords Dynamics · Non-linear · Artificial damping · Beams

M. Saje, M. Gams, I. Planinc
Faculty of Civil and Geodetic Engineering
Jamova 2, 1000 Ljubljana, Slovenia
Tel.: +386-1-47-68-613
Fax: +386-1-47-68-629
E-mail: msaje@fgg.uni-lj.si

1 Introduction

The controllable dissipation of high frequencies in the time integration of linear and non-linear structural dynamics is not a privilege but a necessity. The issue has been studied and much resolved in linear dynamics (see, e.g. the surveying article by Fung [10]), while the work in the non-linear dynamics is still in progress.

As reported by Kuhl and Crisfield [18], the stability is a key issue in non-linear dynamics. There are three main-stream groups of algorithms, which aim to satisfy the stability criterion of the energy conservation/decay. The first group of algorithms comprises numerical dissipation algorithms for the linear dynamics. These al-

gorithms do not guarantee dissipation of energy in the non-linear regime, and energy in a time step can be created instead of dissipated (see, e.g. [8; 9]).

The second group of algorithms uses the enforced constraint methodology, where energy or momenta conservation requirements are introduced via the Lagrange multiplier method. The approach conserves energy perfectly, but problems with stability of integration may still appear, as discovered by Kuhl and Ramm [19]. Hence, the main focus of research seems to rest on the third group of algoritms, the so-called 'Energy-Momentum Methods (EMM)'.

The conservation of energy and momenta in Energy-Momentum methods is algoritmic in the sense that the algorithm inherently conserves these quantities, and the stability of the algorithm is unchallenged by the above mentioned groups of algorithms. The earliest schemes employing the EMM methodology were proposed by Simo *et al.* [28]. The concept has been widely adopted and applied to a variety of problems. Another advantage of the algorithm is the ease with which it can be modified to include a *guaranteed* numerical dissipation. Various modifications of the method have been developed to include the dissipation [1; 2; 8; 15; 18; 25]. The contribution of the present paper is also aimed at this area of research.

In addition to the three main groups of algorithms mentioned above, a subgroup could be identified, which introduces Lagrange multipliers for imposing kinematic constraints resulting in a set of differential-algebraic equations, which renders the system stiff by default, as the frequencies associated with algebraic equations are infinite. A number of approaches for integration of these equations have been presented, see, e.g. [3; 4; 6; 11; 16]. Similarly, Betsch and Steinmann [5] treated the mechanical system as constrained from the onset, resulting in a formulation with greater number of multipliers than in other formulations.

The performance of the present energy decaying approach is demonstrated in conjunction with the energy and momenta conserving method by Gams *et al.* [11] for the planar Reissner [22] beam. The method is essentially a modified version of the Energy-Momentum method, in which the kinematic constraints are satisfied 'weakly' and strains updated incrementally, resulting in an inherent energy and momenta conservation.

The idea of using rate form of the strain-displacement relations to achieve energy and momenta conservation was originally developed by Sansour *et al.* [23] for shell formulations. It was applied to cases of classical and chaotical motion of shells as well as cases of dynamic stability [24]. Futhermore, Sansour *et al.* recently extended the approach to arbitrary continuum formulations [26], which is a generalization of the method presented in Gams *et al.* [11].

The present approach for damping high frequencies uses a viscosity-type damping on strains [1; 2; 25]. The novelty of the approach is applying the damping only at places where it is needed and at times when it is needed.

To this end a heuristic algorithm is proposed for identification of such places, and a special scaling function for damping to smoothen the transition between damped and undamped phases. The proposed heuristic concept for damping high frequencies is, however, entirely general and applicable in conjunction with any time-stepping integration scheme.

The outline of the paper is as follows. In the next section, an energy conserving scheme for geometrically exact planar beams is briefly presented. The scheme serves as a platform for testing the novel concepts of numerical damping, presented in Sect. 3. In Sect. 4 the scheme is thoroughly tested on a set of representative numerical simulations, featuring both highly and moderately stiff systems.

2 Energy conserving scheme

2.1 The planar Reissner beam [22]

An initially straight planar elastic beam of initial length L in the (x, y)-plane of a spatial Cartesian coordinate system (x,y,z) with base vectors $\mathbf{e}_x$, $\mathbf{e}_y$ and $\mathbf{e}_z$ is considered (Fig. 1). The beam is initially rotated with respect to $\mathbf{e}_x$ by an angle φ_0. A material point on the beam centroid axis is identified by the material coordinate, $s \in [0,\ L]$. The cross-sections, associated with the material points, are assumed constant and symmetric with respect to the plane (x, y). The Bernoulli hypothesis holds, with membrane, shear and bending strains being taken into account. The spatial position of an arbitrary material point of the centroid axis, s, is identified by spatial coordinates $x(s)$ and $y(s)$.

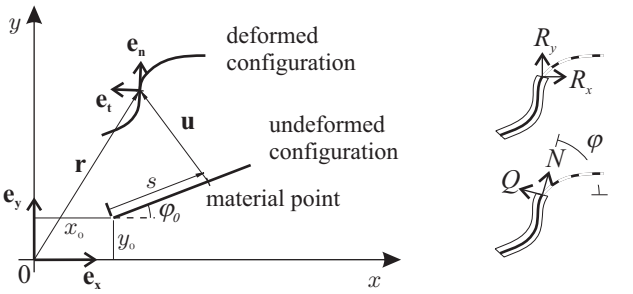

Fig. 1 Beam configurations, left. Notation of stress resultants, right.

2.2 Kinematics of the beam

The kinematic equations of the beam are given by

$$\boldsymbol{\epsilon} = \boldsymbol{\Lambda}\left(\mathbf{u} + \mathbf{x}\right)' + \mathbf{c}_1, \tag{1}$$

where $\boldsymbol{\epsilon}$ is the strain vector, $\mathbf{u}$ the displacement vector and $\mathbf{x}$ the initial position vector of the centroid axis. $\boldsymbol{\Lambda}$ is the rotation matrix and $\mathbf{c}_1$ is a given vector constant:

$$\boldsymbol{\epsilon} = \begin{bmatrix} \varepsilon \\ \gamma \\ \kappa \end{bmatrix},\ \mathbf{u} = \begin{bmatrix} u \\ v \\ \varphi \end{bmatrix},\ \mathbf{x} = \begin{bmatrix} x_0 + s\cos\varphi_0 \\ y_0 + s\sin\varphi_0 \\ 0 \end{bmatrix},$$

$$\boldsymbol{\Lambda} = \begin{bmatrix} \cos\varphi & \sin\varphi & 0 \\ -\sin\varphi & \cos\varphi & 0 \\ 0 & 0 & 1 \end{bmatrix},\ \mathbf{c}_1 = \begin{bmatrix} -1 \\ 0 \\ 0 \end{bmatrix}.$$

ε, γ and κ are axial, shear and bending strain, respectively; u and v are the x and y components of the displacement vector and φ is the rotation. The prime ($'$) denotes differentiation with respect to s.

2.3 Principle of virtual work

The principle of virtual work of the beam is given by:

$$\int_0^L \left[\mathbf{N}^{\mathrm{T}}\,\delta\boldsymbol{\epsilon} - (\mathbf{p}^{\mathrm{T}} - \ddot{\mathbf{u}}^{\mathrm{T}}\,\mathbf{c}_\rho\,)\,\delta\mathbf{u}\right]\mathrm{d}s - \mathbf{P}^{\mathrm{T}}\,\delta\boldsymbol{\Psi} = 0. \qquad (2)$$

Here $\mathbf{N}$ is the vector of stress resultants in the local basis $(\mathbf{e}_n, \mathbf{e}_t, \mathbf{e}_z)$, $\mathbf{p}$ is the vector of external distributed loads (given per unit length of the undeformed axis), $\mathbf{c}_\rho$ is the diagonal matrix of cross-sectional inertial properties, $\mathbf{P}$ is the vector of generalized boundary loads and $\boldsymbol{\Psi}$ is the vector of generalized boundary displacements:

$$\mathbf{N} = \begin{bmatrix} N \\ Q \\ M \end{bmatrix},\ \mathbf{c}_\rho = \mathrm{diag}(A\rho, A\rho, I\rho),\ \mathbf{p} = \begin{bmatrix} p_x \\ p_y \\ m_z \end{bmatrix},$$

$$\mathbf{P}^{\mathrm{T}} = [P_1,\, P_2,\, P_3,\, P_4,\, P_5,\, P_6]\,,$$

$$\boldsymbol{\Psi}^{\mathrm{T}} = [u(0),\, v(0),\, \varphi(0),\, u(L),\, v(L),\, \varphi(L)]\,.$$

In the case of an elastic material, $\mathbf{N}$ takes a simple form:

$$\mathbf{N} = \mathbf{c}_E\ \boldsymbol{\epsilon} = \mathrm{diag}(EA, GA_{\mathrm{S}}, EI)\,\boldsymbol{\epsilon}.$$

E and G are elastic and shear moduli, A and A_{S} are the area and the shear area of the cross-section of the beam, and I is its moment of inertia; ρ is density of material; δ denotes variation; a superposed dot denotes the differentiation with respect to time.

$\delta\boldsymbol{\epsilon}$ in Eq. (2) is obtained by the variation of Eq. (1), i.e. $\delta\boldsymbol{\epsilon} = \delta\left[\boldsymbol{\Lambda}\,(\mathbf{u}+\mathbf{x})' + \mathbf{c}_1\right]$. Inserting the resulting variation into Eq. (2) yields

$$\begin{aligned}&\int_0^L [\mathbf{N}^{\mathrm{T}}\,\boldsymbol{\Lambda}\,\delta\mathbf{u}' + \mathbf{N}^{\mathrm{T}}\,\delta\boldsymbol{\Lambda}\,(\mathbf{u}+\mathbf{x})' \\ &-(\mathbf{p}^{\mathrm{T}} - \ddot{\mathbf{u}}^{\mathrm{T}}\mathbf{c}_\rho)\,\delta\mathbf{u}]\,\mathrm{d}s - \mathbf{P}^{\mathrm{T}}\,\delta\boldsymbol{\Psi} = 0.\end{aligned} \qquad (3)$$

By introducing an auxiliary matrix

$$\mathbf{Y} = \begin{bmatrix} -\sin\varphi & \cos\varphi & 0 \\ -\cos\varphi & -\sin\varphi & 0 \\ 0 & 0 & 0 \end{bmatrix},$$

we can rewrite Eq. (3) as

$$\begin{aligned}&\int_0^L [\mathbf{R}^{\mathrm{T}}\,\delta\mathbf{u}' + \mathbf{Z}^{\mathrm{T}}\,(\mathbf{u}+\mathbf{x})'\,\delta\varphi \\ &-(\mathbf{p}^{\mathrm{T}} - \ddot{\mathbf{u}}^{\mathrm{T}}\,\mathbf{c}_\rho)\,\delta\mathbf{u}]\,\mathrm{d}s - \mathbf{P}^{\mathrm{T}}\,\delta\boldsymbol{\Psi} = 0,\end{aligned} \qquad (4)$$

where

$$\mathbf{R}^{\mathrm{T}} = \mathbf{N}^{\mathrm{T}}\,\boldsymbol{\Lambda} = [R_x,\, R_y,\, M]$$

are the stress resultants with respect to the spatial basis (Fig. 1), and

$$\mathbf{Z}^{\mathrm{T}} = \mathbf{N}^{\mathrm{T}}\,\mathbf{Y} = [-R_y,\, R_x,\, 0]\,.$$

The principle in Eq. (4) is ready for the application of a displacement-based finite element formulation, as it only includes variations of displacements.

2.4 Hamilton's principle

The virtual work principle given in Eq. (4) is integrated over the time interval $[t_n, t_{n+1}]$ to obtain Hamilton's principle for the beam

$$\begin{aligned}&\int_{t_n}^{t_{n+1}} \{\int_0^L [\mathbf{R}^{\mathrm{T}}\,\delta\mathbf{u}' + \mathbf{Z}^{\mathrm{T}}\,(\mathbf{u}+\mathbf{x})'\,\delta\varphi \\ &-(\mathbf{p}^{\mathrm{T}} - \ddot{\mathbf{u}}^{\mathrm{T}}\mathbf{c}_\rho)\,\delta\mathbf{u}]\,\mathrm{d}s - \mathbf{P}^{\mathrm{T}}\,\delta\boldsymbol{\Psi}\}\,\mathrm{d}t = 0.\end{aligned} \qquad (5)$$

The same integration is applied to the kinematic equations in the time rate form:

$$\int_{t_n}^{t_{n+1}} \dot{\boldsymbol{\epsilon}}\,\mathrm{d}t = \int_{t_n}^{t_{n+1}} \left[\dot{\boldsymbol{\Lambda}}\,(\mathbf{u}+\mathbf{x})' + \boldsymbol{\Lambda}\,(\mathbf{u}')^{\cdot}\right]\mathrm{d}t. \qquad (6)$$

The reason for taking the rate, i.e. the weak form rather than the strong form is described in [11]. Finally, the time integration of constitutive equations is performed:

$$\int_{t_n}^{t_{n+1}} \mathbf{N}\,\mathrm{d}t = \int_{t_n}^{t_{n+1}} \mathbf{c}_E\,\boldsymbol{\epsilon}\,\mathrm{d}t. \tag{7}$$

2.5 Time discretization (midpoint scheme)

For the time discretization of Hamilton's principle, Eq. (5), and its adjoined set of the constraining kinematic and constitutive equations (6) and (7), we use the following midpoint approximation rules:

$$\int_{t_n}^{t_{n+1}} f(t)\,\mathrm{d}t \approx f(t_m)\,\Delta t, \tag{8}$$

$$\dot{f}_m \approx \frac{f_{n+1}-f_n}{\Delta t} = \frac{\Delta f}{\Delta t}, \tag{9}$$

$$\ddot{f}_m \approx \frac{\dot{f}_{n+1}-\dot{f}_n}{\Delta t} = \frac{\Delta \dot{f}}{\Delta t}, \tag{10}$$

where

$$t_m = \frac{1}{2}(t_n + t_{n+1}),$$

$$\Delta t = t_{n+1} - t_n.$$

'f' refers to an arbitrary function of t. Subscript 'm' refers to the midpoint configuration at $t_m = t_n + \frac{1}{2}\Delta t$, '$n$' to that at t_n and '$n+1$' to the one at $t_{n+1} = t_n + \Delta t$.

The application of the midpoint rules to Eq. (5) yields

$$\begin{aligned}&\{\int_0^L [\mathbf{R}_m^{\mathrm{T}}\,\delta\mathbf{u}'_m + \mathbf{Z}_m^{\mathrm{T}}\,(\mathbf{u}+\mathbf{x})'_m\,\delta\varphi_m \\ &-(\mathbf{p}^{\mathrm{T}} - \ddot{\mathbf{u}}^{\mathrm{T}}\mathbf{c}_\rho)_m\,\delta\mathbf{u}_m]\,\mathrm{d}s - \mathbf{P}_m^{\mathrm{T}}\,\delta\boldsymbol{\Psi}_m\}\,\Delta t = 0.\end{aligned} \tag{11}$$

The midpoint time integration of kinematic equations (6) gives

$$\begin{aligned}&\int_{t_n}^{t_{n+1}} \dot{\boldsymbol{\epsilon}}\,\mathrm{d}t \approx \dot{\boldsymbol{\epsilon}}_m\,\Delta t \\ &= \left[\,\dot{\boldsymbol{\Lambda}}\,(\mathbf{u}+\mathbf{x})' + \boldsymbol{\Lambda}\,(\mathbf{u}')^{\cdot}\,\right]_m \Delta t.\end{aligned}$$

As $\dot{\boldsymbol{\epsilon}}_m\,\Delta t = \Delta\boldsymbol{\epsilon}$ by Eq. (9), this yields

$$\begin{aligned}\Delta\boldsymbol{\epsilon} &= \mathbf{Y}_m\,(\mathbf{u}+\mathbf{x})'_m\,\dot{\varphi}_m\,\Delta t + \boldsymbol{\Lambda}_m(\mathbf{u}')^{\cdot}_{\mathbf{m}}\Delta t \\ &= \mathbf{Y}_m\,(\mathbf{u}+\mathbf{x})'_m\,\Delta\varphi + \boldsymbol{\Lambda}_m\,\Delta\mathbf{u}'.\end{aligned} \tag{12}$$

Note that matrices $\boldsymbol{\Lambda}_m = \boldsymbol{\Lambda}(\varphi_m)$ and $\mathbf{Y}_m = \mathbf{Y}(\varphi_m)$ are consistently evaluated at the midpoint configuration rather than by the trapezoidal rule. This way the orthogonality of the rotation operator preserved. The midpoint time integration of the constitutive equations (7) results in their standard form:

$$\int_{t_n}^{t_{n+1}} \mathbf{N}\,\mathrm{d}t = \int_{t_n}^{t_{n+1}} \mathbf{c}_E\,\boldsymbol{\epsilon}\,\mathrm{d}t \Rightarrow \mathbf{N}_m = \mathbf{c}_E\;\boldsymbol{\epsilon}_m. \tag{13}$$

2.6 Energy conservation

The mechanical energy (Π) of the deformed, yet unloaded beam at a specific time is the sum of the strain and kinetic energies

$$\Pi = \frac{1}{2}\int_0^L \left(\boldsymbol{\epsilon}^{\mathrm{T}}\,\mathbf{c}_E\;\boldsymbol{\epsilon} + \dot{\mathbf{u}}^{\mathrm{T}}\,\mathbf{c}_\rho\,\dot{\mathbf{u}}\right)\,\mathrm{d}s.$$

The change of the mechanical energy between two consecutive time stations, t_n and t_{n+1}, is

$$\begin{aligned}\Delta\Pi = \frac{1}{2}\int_0^L &\left(\boldsymbol{\epsilon}_{n+1}^{\mathrm{T}}\,\mathbf{c}_E\;\boldsymbol{\epsilon}_{n+1} - \boldsymbol{\epsilon}_n^{\mathrm{T}}\,\mathbf{c}_E\;\boldsymbol{\epsilon}_n\right. \\ &\left. + \dot{\mathbf{u}}_{n+1}^{\mathrm{T}}\,\mathbf{c}_\rho\,\dot{\mathbf{u}}_{n+1} - \dot{\mathbf{u}}_n^{\mathrm{T}}\mathbf{c}_\rho\,\dot{\mathbf{u}}_n\right)\,\mathrm{d}s.\end{aligned}$$

The differences of the squares of $\boldsymbol{\epsilon}$ and $\dot{\mathbf{u}}$ are rewritten as:

$$\frac{1}{2}(\boldsymbol{\epsilon}_{n+1}^2 - \boldsymbol{\epsilon}_n^2) = \frac{\boldsymbol{\epsilon}_{n+1}^{\mathrm{T}} + \boldsymbol{\epsilon}_n^{\mathrm{T}}}{2}(\boldsymbol{\epsilon}_{n+1} - \boldsymbol{\epsilon}_n) = \boldsymbol{\epsilon}_m^{\mathrm{T}}\,\Delta\boldsymbol{\epsilon},$$

$$\frac{1}{2}(\dot{\mathbf{u}}_{n+1}^2 - \dot{\mathbf{u}}_n^2) = \frac{\dot{\mathbf{u}}_{n+1}^{\mathrm{T}} + \dot{\mathbf{u}}_n^{\mathrm{T}}}{2}(\dot{\mathbf{u}}_{n+1} - \dot{\mathbf{u}}_n) = \dot{\mathbf{u}}_m^{\mathrm{T}}\,\Delta\dot{\mathbf{u}}.$$

$\boldsymbol{\epsilon}_m$ and $\dot{\mathbf{u}}_m$ denote the midpoint values of $\boldsymbol{\epsilon}$ and $\dot{\mathbf{u}}$ evaluated by the trapezoidal rule. The product of the velocities is further modified

$$\dot{\mathbf{u}}_m^{\mathrm{T}}\ \Delta\dot{\mathbf{u}} = \frac{\Delta\mathbf{u}^{\mathrm{T}}}{\Delta t}\,\ddot{\mathbf{u}}_m\,\Delta t = \ddot{\mathbf{u}}_m^{\mathrm{T}}\,\Delta\mathbf{u}.$$

In the last step, $\frac{\dot{\mathbf{u}}_{n+1}+\dot{\mathbf{u}}_n}{2} = \frac{\Delta\mathbf{u}}{\Delta t}$ was assumed, which also gives the velocity update for the scheme

$$\dot{\mathbf{u}}_{n+1} = 2\frac{\Delta\mathbf{u}}{\Delta t} - \dot{\mathbf{u}}_n.$$

With the help of Eq. (13) the energy change in a time step becomes

$$\Delta\Pi = \int_0^L \left(\mathbf{N}_m^{\mathrm{T}}\,\Delta\boldsymbol{\epsilon} + \ddot{\mathbf{u}}_m^{\mathrm{T}}\,\mathbf{c}_\rho\,\Delta\mathbf{u}\right)\,\mathrm{d}s. \tag{14}$$

The strain increments are substituted by the expression given in Eq. (12), leading to

$$\begin{aligned}\Delta\Pi = \int_0^L [&\mathbf{N}_m^{\mathrm{T}}\,\mathbf{Y}_m\,(\mathbf{u}+\mathbf{x})'_m\,\Delta\varphi \\ &+\mathbf{N}_m^{\mathrm{T}}\,\boldsymbol{\Lambda}_m\,\Delta\mathbf{u}' + \ddot{\mathbf{u}}_m^{\mathrm{T}}\,\mathbf{c}_\rho\,\Delta\mathbf{u}]\,\mathrm{d}s,\end{aligned} \tag{15}$$

or in the abbreviated form

$$\begin{aligned}\Delta\Pi = \int_0^L [&\mathbf{R}_m^{\mathrm{T}}\,\Delta\mathbf{u}' + \mathbf{Z}_m^{\mathrm{T}}\,(\mathbf{u}+\mathbf{x})'_m\,\Delta\varphi \\ &+\ddot{\mathbf{u}}_m^{\mathrm{T}}\,\mathbf{c}_\rho\,\Delta\mathbf{u}]\,\mathrm{d}s.\end{aligned} \tag{16}$$

After we eliminate the external loading terms from Eq. (11) and compare the result with Eq. (16), we see that the expressions in equations are virtually the same, with the differences being that (i) in Eq. (11) we have infinitesimal variations, while in Eq. (16) there are changes in u, v and φ; and (ii) Eq. (11) represents the principle of virtual work and thus identically equals to zero for any virtual displacements, while Eq. (16) only represents the change of energy at two consecutive time stations, which generally does not vanish for any finite-size increments of generalized displacements. If, however, the principle of virtual work is satisfied indeed, it is easy to show that Eq. (16) also vanishes for any $\Delta\mathbf{u}$, related to $\Delta\boldsymbol{\epsilon}$ by Eq. (12). This yields $\Delta\Pi = 0$, and, consequently, the conservation of the energy in the time step.

3 Numerical damping

3.1 Concepts

Many time-integration schemes with damping have been developed and extensively used so far [7; 13; 15]. Their primary goal is to filter out high frequencies of the response, which, in turn, increases the stability of solution. They are used both in energy non-conserving and conserving schemes. In fact, the response of any energy conserving scheme inherently includes high frequencies, which often yields physically unreasonable solutions [11; 15]. Finding a computationally effective damping procedure, which truly affects only the highest modes, is the Holy Grail of the non-linear dynamics. The solution we are about to present is aimed towards this goal.

The main idea behind the proposed approach is to apply damping at places where it is needed, at times when it is needed, and doing so at as low numerical cost as possible. Another peculiarity of the present approach is the use of a non-linear damping, the issue not often met in literature. Its aim is a numerical smoothness, which will be addressed later in the text. Damping is applied

to strains (in a similar way as in [1], [2] or [25]), rather than to both displacements and strains as in [15], where damping of both strains and displacements is advocated to assure energy decay in the case of very small or vanishing deformations. Such an argumentation is in contrast with present formulation, where damping is disengaged if the rate of deformations is small, as is explained in Sect. 3.3.

The need for damping is identified in the strain space, because the high frequencies are usually easier to identify in the strain rather than in the displacement space. Another reason for applying damping to strains only is that the displacements are already indirectly affected by damping of the strains. The concept of identification is empirical by origin, and its physical aspects are purposely neglected.

The approach will be combined with the energy conserving scheme presented in Sect. 2 (or in more a detail in [11]), yet it is by no means restricted to this particular formulation. The concept is in fact entirely general, and can be used without further contemplation in any displacement-based formulation.

3.2 Theory

As mentioned in Sect. 3.1, the damping is directly enforced only to strains:

$$\boldsymbol{\epsilon}_m^* = \frac{1}{2}(\boldsymbol{\epsilon}_n + \boldsymbol{\epsilon}_{n+1}) + \alpha\, g\left(\dot{\boldsymbol{\epsilon}}_m\right). \tag{17}$$

Here α presents the magnitude of damping and g stands for an arbitrary sign preserving function. Using the midpoint rule we write

$$\boldsymbol{\epsilon}_m^* = \boldsymbol{\epsilon}_m + \alpha\, g\left(\frac{\Delta\boldsymbol{\epsilon}}{\Delta t}\right). \tag{18}$$

The change of energy in a time step in absence of external forces is now (following from Eq. (14)):

$$\begin{aligned} 0 &= \int_0^L \left(\left(\mathbf{c}_E\ \boldsymbol{\epsilon}_m^*\right)^{\mathrm{T}} \Delta\boldsymbol{\epsilon} + \ddot{\mathbf{u}}_m^{\mathrm{T}}\ \mathbf{c}_\rho\, \Delta\mathbf{u} \right) \mathrm{d}s \\ 0 &= \int_0^L \left(\left(\mathbf{c}_E\ \boldsymbol{\epsilon}_m\right)^{\mathrm{T}} \Delta\boldsymbol{\epsilon} + \ddot{\mathbf{u}}_m^{\mathrm{T}}\ \mathbf{c}_\rho\, \Delta\mathbf{u} \right) \mathrm{d}s \\ &\quad + \int_0^L \alpha \left(\mathbf{c}_E\, g\left(\tfrac{\Delta\boldsymbol{\epsilon}}{\Delta t}\right)\right)^{\mathrm{T}}\ \Delta\boldsymbol{\epsilon}\, \mathrm{d}s. \end{aligned} \tag{19}$$

While we have already established that the first row of Eq. (19) equals $\Delta\Pi$, we can rewrite the second one by introducing a modified scalar function $\tilde{g}$, which still preserves the sign of the argument

$$0 = \Delta\Pi + \int_0^L \alpha\, \tilde{g}\left(\Delta\,\boldsymbol{\epsilon}^2\right)\, \mathrm{d}s.$$

Hence, the mechanical energy in a time step is dissipated for any $\alpha > 0$.

3.3 Algorithm

As mentioned in Sect. 3.1, we desire to apply damping at places where it is most needed, at the time when it is needed. Locations of practical interest are the integration points. As there can be many of them, the algorithm for identifying the need for damping must be computationally as effective as possible. The following procedure is proposed: the analysis starts without damping. In each time step at every integration point, the signs of the last

$\tilde{\gamma}$ changes of strains are observed (at least one of these changes must, however, be larger than a prescribed value τ). If they form a repeated sequence of pluses and minuses in a perfect saw-like pattern, damping is engaged. With damping engaged, again, in each time step, the signs of the last $\tilde{\delta}$ changes are observed. If they are either all positive or all negative, the damping is disengaged. Also, if all $\tilde{\delta}$ actual changes of strains are smaller than a prescribed value τ, the damping is disengaged. After the damping is disengaged, the routine starts over testing whether damping should be engaged again. Both situations are schematically presented in Fig. 2.

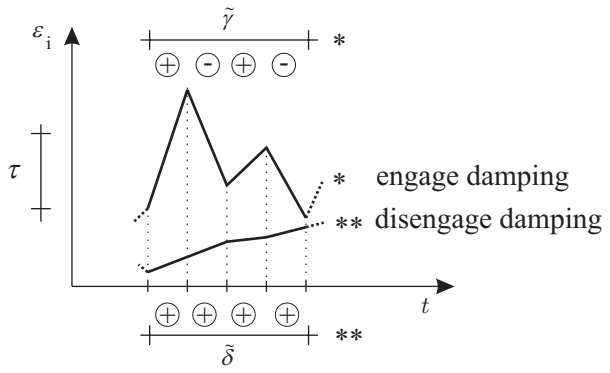

Fig. 2 Schematic drawings of situtaions indicating damping should be engaged or disengaged.

The value of the threshold τ is by no means arbitrary. Prior to the analysis, we choose the precision of the internal forces. Oscillations beyond these values will be considered as a potential noise, and will be, if so determined by the identifying algorithm, damped. The chosen values are divided by the corresponding stiffnesses ($\mathbf{c}_E$) to obtain the thresholds for the corresponding strains.

$\tilde{\gamma}$ and $\tilde{\delta}$ present the number of observed signs of strain increments (see Fig. 2, where $\tilde{\gamma} = \tilde{\delta} = 4$). Values of these parameters are measures of strictness regarding the start or the end of damping. There is no upperlimit, while the theoretical lower limit is two. The range of values for $\tilde{\gamma}$ and $\tilde{\delta}$ from four to ten is reasonable. They need not be equal.

The only restriction imposed on the damping function g is that it is sign preserving. Nevertheless we only have three conceptually different choices : (i) an odd power type, (ii) a linear function or (iii) an arctan type of function.

The odd power type function should, in principle, be the most aggressive toward the high frequency content, but in practice its aggression is also its pitfall. Damping is found to be too intensive and leads to either too strong damping or to a loss of convergence of the Newton-Raphson method at the onset of the damping phase. The linear function is the most commonly preferred function in the computational community, largely due to simplicity of theoretical deductions, as damping formulations are rarely as simple as the one given in Sect. 3.2. The arctan type of function sets an upper limit on the amount of damping, which increases the stability of the Newton-Raphson procedure in transitions between the damped and undamped phases, and is therefore the choice of preference in our analyzes.

In fact, further parameter β is introduced into the damping function, which smoothens the transition even

further:

$$g(\dot{\boldsymbol{\epsilon}}_m) = \arctan\left(\frac{\dot{\boldsymbol{\epsilon}}_m}{\beta}\right).$$

3.4 Unexplored options

One might justifiably argue that the price of the algorithm might still be too high for *extremely* large systems, as more memory is demanded to monitor the strain history and identify the oscillations. In those cases room is still left to simplify further the proposed algorithm. For example, one might decide in advance, where in the system the artificial damping is allowed, and disable it in other locations. In this way enormous savings might be achieved. Another option would allow damping to work only on one kind of strains, effectively cutting the computer memory requirement to one third. These approaches and their effects are, however, not analyzed further in this paper.

4 Numerical simulations

The computer code was generated entirely in an automatic code generating environment AceGen [17], which is able to produce the finite element code in various programming languages. The actual computations were performed in MATLAB [20]. In order to avoid locking, the reduced numerical integration was used for the stiffness part, whereas full integration was used in inertia terms. The formulation sets no restrictions regarding the order of spatial interpolation. In all numerical cases presented here, the quadratic elements are used.

4.1 The swinging pendulum

This example, leading to a highly stiff system of differential equations, was originally proposed by Bauchau *et al*. [3; 4], and subsequently analyzed by Ibrahimbegović and co-workers [14; 15; 16]. The pendulum consists of a flexible beam hinged at both ends into two rigid links (Fig. 3). The rigid links impose a kinematic constraint corresponding to fixed distance between points O_1 and A, and O_2 and E.

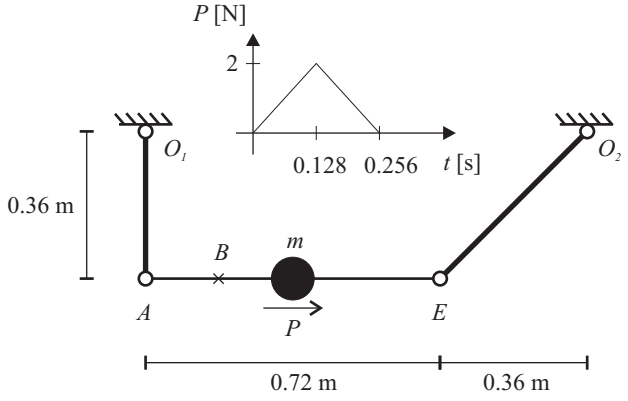

Fig. 3 The swinging pendulum: geometry and load data.

A point mass $m = 0.5\,\mathrm{kg}$ is rigidly connected to the flexible beam at its mid-span. Point B is the observation point. The material and geometric properties of the

flexible beam are:

$$E = 73 \cdot 10^9\,\mathrm{N/m^2},\ A = 0.005 \cdot 0.001\,\mathrm{m^2},$$
$$L = 0.72\,\mathrm{m},\ I = \frac{1}{12} \cdot 0.005 \cdot 0.001^3\,\mathrm{m^4},$$
$$\rho = 2700\,\mathrm{kg/m^3},\ m_{\mathrm{BEAM}} = 0.00972\,\mathrm{kg}.$$

Shear strains are made negligible by setting a large value for the shear modulus ($G = 100\,E$). As in [3] and [14] the rigid links are assumed weightless ($\rho = 0$ kg/m^3) and their rigidity is modelled by assuming large Young's modulus, i.e. ten times the value of the modulus of the flexible beam. A time step $\Delta t = 0.0005$ s is used. Four finite elements were used to model each rigid link and eight finite elements for modelling the flexible beam.

The system is initially at rest. It is set in motion by a horizontal time-dependent pulse at the mid-span of the beam. The time variation of the pulse intensity is shown in Fig. 3. After the pulse vanishes at $t = 0.256\,\mathrm{s}$, the system is left to oscillate freely.

At first, the links are rotating in the counter-clock-wise direction. At $t \approx 0.64\,\mathrm{s}$, the right link reverses its direction and starts rotating clock-wise. Simultaneously, the horizontal velocity of the point mass changes its direction, which acts almost like an impact on the system. A smooth response dominated by the low frequencies abruptly changes into a complicated high frequency response. This event, however, does not perturb predominantly swinging motion, but plagues it by high frequencies of internal forces [11; 14; 15].

The case is calculated with three different settings of the damping parameters. The undamped case ($\alpha = 0$), the slightly damped case ($\alpha = 0.01$, $\beta = 100$, $\tilde{\gamma} = \tilde{\delta} = 5$), and the moderately damped case ($\alpha = 0.1$, $\beta = 100$, $\tilde{\gamma} = \tilde{\delta} = 5$). The changes greater than 0.01 N or 0.00001 Nm are considered as the numerical threshold for internal forces and the bending moment, respectively. Fig. 4 depicts the solution over the entire time domain. The comparison between the three solutions (undamped, slightly and moderately damped) is impossible on that scale, and so two magnifications are provided in Fig. 5. Only there can we recognize the differences and analyze results. It is clear that the slightly damped solution follows the undamped one quite closely, and only a slightly smoother response in the displacement domain is obtained, while the moderately damped solution provides significantly smoother solution. Both damped solutions obviously preserve principal low-order frequency periods of the solution, just as in Bauchau and Theron [4], but unlike as in Ibrahimbegović *et al.* [15].

The effect of damping (Fig. 6) on the total energy is very interesting, as it shows that only a very limited amount of energy has been dissipated, which is especially true for the case with $\alpha = 0.01$. Futhermore, it reveals that the rate of energy decay appears to diminish with time, which is desired.

Fig. 7 depicts areas od damping in time/space domain. Dark areas mark damping. It can clearly be seen, that most of damping takes place in the 'central' flexible

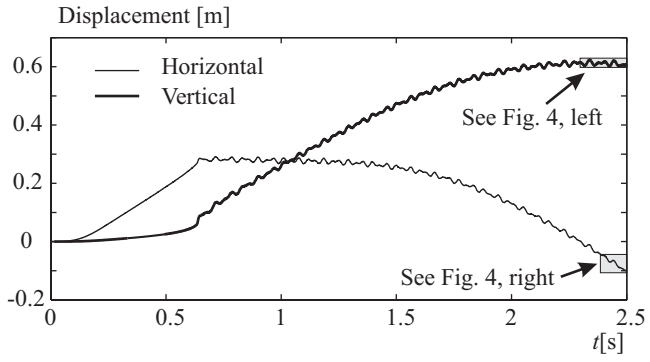

Fig. 4 Swinging pendulum. Horizonal and vertical displacements of point B.

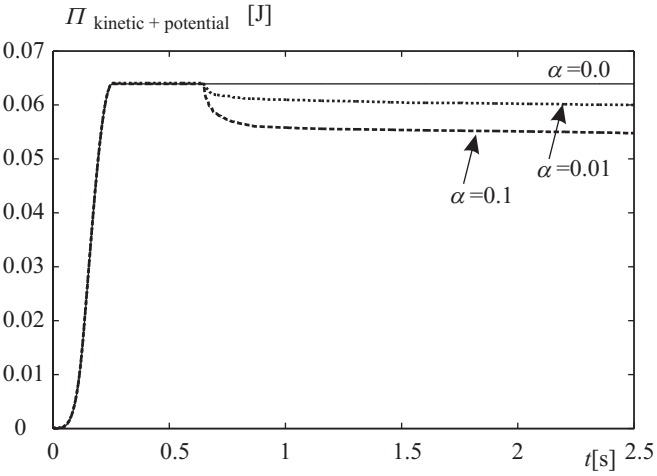

Fig. 6 Swinging pendulum. The effect of damping on energy. $\tilde{\gamma} = \tilde{\delta} = 5$.

part of the beam, whereas damping in rigid links is only due to axial deformations. There appears to be hardly any damping at all due to the bending strains. Even though the rate of damping reduces with time, there is no indication it may ever stop. The results in Fig. 7 suggest some reduction of damping with time, but not on the scale presented in Fig. 6. This is due to the reduction of velocities with time, which in turn reduces the (velocity proportional) damping.

While the picture in Fig. 7 may be interesting to look at, and some insight is indeed given into where the most oscillatory response appears, it is only a byproduct of the analysis. The main focus should remain on displacements and the internal forces, the latter are presented and analyzed in Fig. 8.

Once damping is applied, the internal forces become more 'reasonable', as the high frequencies are filtered out. The most problematic among the internal forces are the axial forces. The noise is filtered out by both damping cases. The shear forces are by far not as problematic, because their maximal values are so much smaller compared to the maximal values in the axial force, and even the undamped solution is not entirely unacceptable. The response of the undamped bending moments is also very oscillatory. This is remedied with the damping case $\alpha = 0.01$ already, which can be seen if Fig. 8 is magnified (not presented here). The damping case with $\alpha = 0.1$ further smoothens the response. Please observe again from Fig. 5 how little effect the damping has on the response of the displacements!

Finally we examine the effect of damping on the frequency spectrum of the internal forces. This is achieved by the Discrete Fourier Transform algorithm, a built-in function of MATLAB [20]. The results, presented in Fig. 9, show that high frequencies are well eliminated by the present energy-decaying scheme. Assuming the rule of

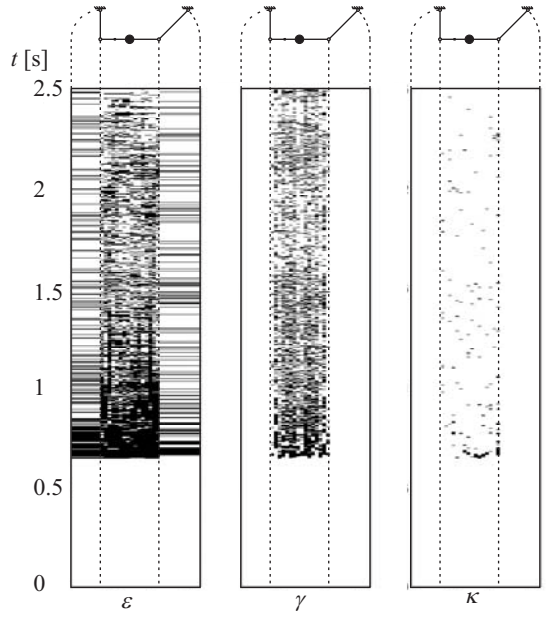

Fig. 7 Swinging pendulum. Damping in time and space for strains ε, γ and κ ($\alpha = 0.01$).

thumb in dynamics, which states that only frequencies of about $(\frac{1}{10}\Delta t)$ or less are consistently taken into account, we can estimate that the frequencies higher than about 200 Hz represent the numerical noise and should be damped out. This rule strictly applies only to the displacements, while the related limit for the strains is not known. It is therefore only a rough estimate. In light of this, it appears that the damping case $\alpha = 0.1$ has damped out too much of the low frequencies, while the damping case $\alpha = 0.01$ has performed outstandingly.

4.2 Planar motion of a multibody system

This example of a stiff dynamical system was first introduced by Ibrahimbegović and Mamouri [14] to demonstrate the versatility of their formulation for dealing with different types of joints. The example is, however, of interest in its own right, since it undergoes interesting configurations, responds in high and low frequencies, and cannot be satisfactorily solved with non-conserving methods, such as the Newmark [21] or HHT-α [13] methods, as was clearly shown in [14].

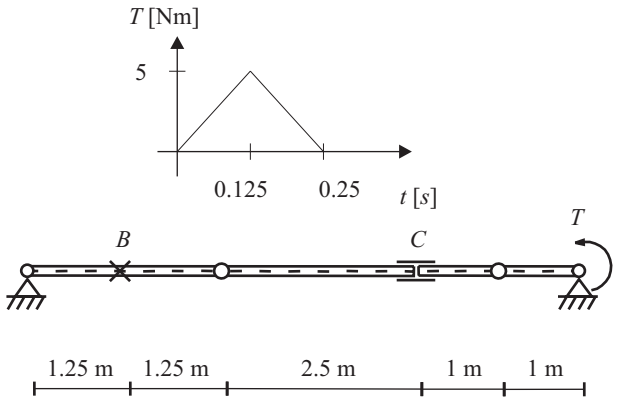

Fig. 10 The multibody system: geometry and load data.

The multibody system under consideration is made of 4 flexible members interconnected by either revolute or prismatic joints (Fig. 10). Point B is the observation point. The system is initially at rest. It is put into motion by a concentrated torque at the right support. The time variation of the torque is depicted in Fig. 10. The system is modeled by 12 quadratic finite elements. The remaining descriptive data are:

$$EA = 5.65 \cdot 10^5\,\mathrm{N},\ GA_\mathrm{S} = 1.4038 \cdot 10^5\,\mathrm{N},$$

$$EI = 3.04 \cdot 10\,\mathrm{Nm}^2,\ A\rho = 1.35 \cdot 10^{-2}\,\mathrm{kg\,m}^{-1},$$

$$I\rho = 1.125 \cdot 10^{-6}\,\mathrm{kgm},\ \Delta t = 0.001\ \mathrm{s}.$$

Again three different settings are used for the computations, the undamped case ($\alpha = 0$), the slightly damped case ($\alpha = 0.0005$, $\beta = 10$, $\tilde{\gamma} = \tilde{\delta} = 5$), and the moderately damped case ($\alpha = 0.001$, $\beta = 10$, $\tilde{\gamma} = \tilde{\delta} = 5$). The numerical threshold for detection of force and moment oscillations is set to 0.1 N and 0.001 Nm.

The displacements in all three cases vary quite a bit, especially in the case with moderate damping (Fig. 11). Because the *correct* solution is unknown, it is necessary to analyze the accompanying energy and internal forces graphs.

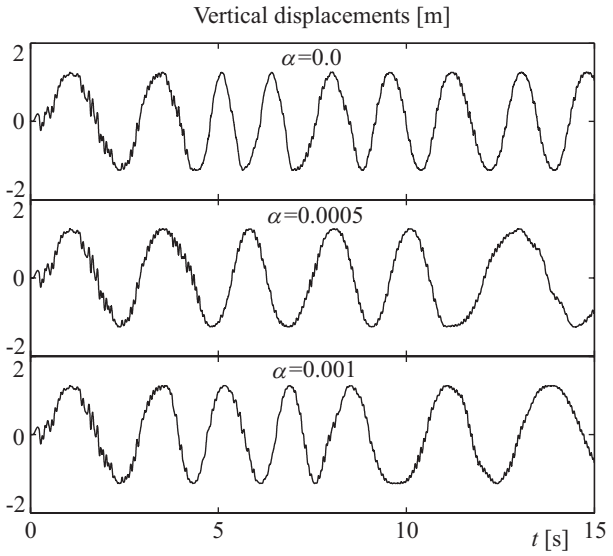

Fig. 11 Multibody system. Vertical displacements at point B.

In Fig. 12, the corresponding graphs of energies are shown. The amount of energy decay in this case is quite high. The scheme with smaller α does not necessarily decay less energy than the one with higher α. The reasons for this are explained in the last paragraph of this section.

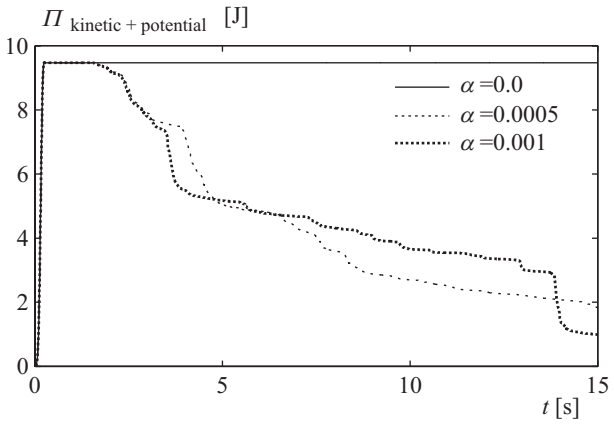

Fig. 12 Multibody system. The effect of damping on energy. $\tilde{\gamma} = \tilde{\delta} = 5$ and $\beta = 10$ in cases with damping.

The internal forces are shown in Fig. 13. One may without a hesitation conclude that the undamped results give erroneous forces, but the choice regarding the correct amount of damping is perhaps not so easy.

Frequency spectrum of the internal forces for all three damping cases are presented in Fig. 14. In this case frequencies higher than 100 Hz could be considered as a numerical noise. Both damping cases deal with the axial force rather efficiently, but the damping with $\alpha = 0.001$ appears to damp the shear force and the bending moment a bit too much.

This case is the toughest in all respects, as the undamped solution gives wrong internal forces. The damped solutions, on the other hand, return reasonable results regarding internal forces, but show considerable differences in the displacements. The difficulties related with

this problem are due to the monotonically growing stiffness of the system with time (which can clearly be seen from the undamped solution for strains in Fig. 13), and coping with such a system is very challenging. Energy corresponding to high frequency oscillations presents a lion's share of total energy, which appears to grow with time. This presents a problem even for the enery preserving schemes, as the amount of high frequency content soars, the Newton-Rapshon procedure is bound to have problems at some point of the analysis. The stiffness of the swinging pendulum case, on the other hand, exhibited a big jump of stiffness, which remained within certain bounds (did not increase with time), and was correspondingly easier to deal with. The reason why the stiffness of the multibody system grows with time while the siffness of the swinging pendulum remains within certain bounds, is purely a consequence of the geometry of both cases.

4.3 The flying spaghetti [27]

In this numerical example, we consider a flexible beam with free ends to be a mechanical model of the flying spaghetti. The beam is initially placed in an inclined position (Fig. 15). The point force and the torque are simultaneously applied to one end of the beam for 2.5 s. Once the loads are removed, the beam continues its free flight. Point B refers to the unloaded end of the beam, and serves as the observation point. The beam is modelled by ten finite elements.

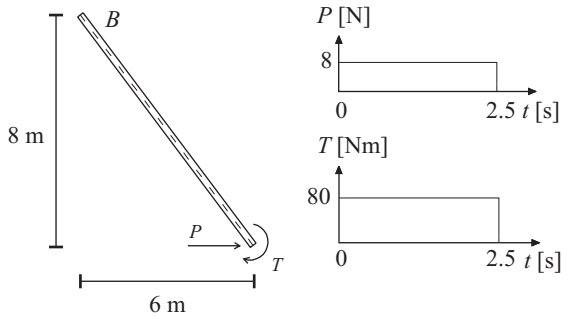

Fig. 15 Flying flexible beam. Geometric and loading data.

Other data regarding the numerical example are:

$$EA = GA_{\mathrm{S}} = 10000\,\mathrm{N},\ EI = 100\,\mathrm{Nm}^2,$$

$$A\rho = 1\,\mathrm{kgm}^{-1},\ I\rho = 10\,\mathrm{kgm},\ \Delta t = 0.1\ \mathrm{s}.$$

This case is computed without damping ($\alpha = 0$), and with slight damping ($\alpha = 0.01$, $\beta = 10$, $\tilde{\gamma} = \tilde{\delta} = 5$). The numerical threshold for detection of force and moment oscillations is set to 0.001 N and 0.00001 Nm, respectively.

The displacements at point B are presented in Fig. 16. We can see that, similarly as in the case of the swinging pendulum, there is a mild smoothening effect of damping on the displacements. The principal frequencies of the response as well as the amplitudes are preserved.

The energy decay is very small relative to the total energy (Fig. 17), and appears to diminish with the increasing time.

Although the effect on the energy decay was practically negligible, the effect onto the internal forces is immense, as can clearly be seen in Fig. 18. The damped solutions give substantially less oscillating results.

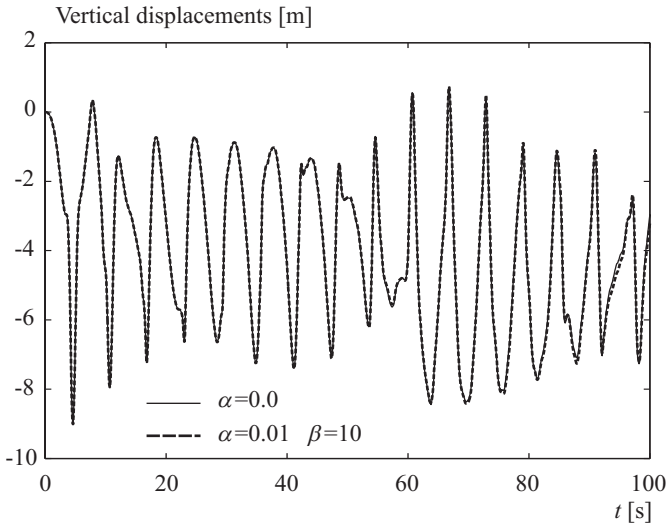

Fig. 16 Flying spaghetti. Vertical displacements at the free end of the beam. $\tilde{\gamma} = \tilde{\delta} = 5$ in the damped case.

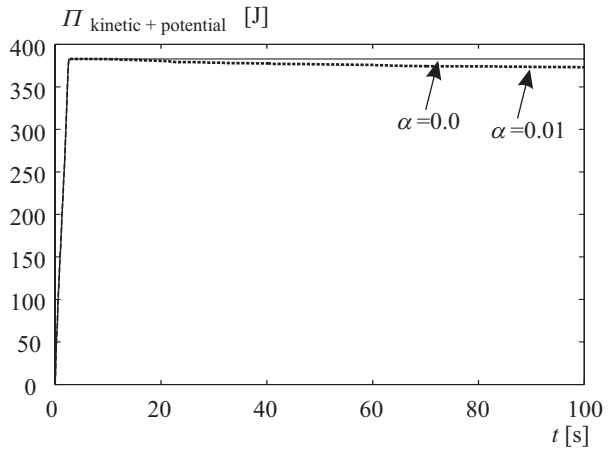

Fig. 17 Flying spaghetti. The effect of damping on energy. $\tilde{\gamma} = \tilde{\delta} = 5$ and $\beta = 10$ in case with damping.

5 Conclusions

A viscous type damping for introducing the controllable numerical dissipation of high frequencies in time integration schemes is enhanced by introducing the idea of applying the dissipation at places, where it is needed, and at times when it is needed, as the principal difference to the usually applied damping schemes. In order to achieve this, a crucial step is the identification of high frequency oscillations. This has been resolved by a simple heuristic identifying algorithm, which monitors the number of recent sign changes of strain increments. Two parameters govern the damping : one controls the magnitude and the other provides a smooth transition between the damping phases.

The methodology is applied in conjunction with an energy conserving formulation for geometrically exact beams, and the algorithm performs extremelly well. As demonstrated with several numerically very demanding cases, it was able to predict accurately the instant, when damping was required, and to damp out the problematic oscillations, while the small and moderate ones remained unaffected. The frequency spectra also show that the principal low order frequencies remain unaffected.

References

1. Armero F, Petőcz E (1999) A new dissipative time-stepping algorithm for frictional contact problems: formulation and analysis. Comput. Methods Appl. Mech. Engrg. 179: 151–178
2. Armero F, Romero I (2003) Energy-dissipative momentum-conserving time-stepping algorithms for the dynamics of nonlinear Cosserat rods. Comput. Mech. 31: 3–26
3. Bauchau OA, Damilano G, Theron NJ (1995) Numerical integration of non-linear elastic multi-body systems. Int.

J. Numer. Methods Engrg. 38: 2737–2751

4. Bauchau OA, Theron NJ (1996) Energy decaying scheme for nonlinear elastic multi-body systems. Comp. Struct. 59: 317–331
5. Betsch P, Steinmann P (2003) Constrained dynamics of geometrically exact beams. Comput. Mech. 31: 49–59
6. Botasso CL, Bauchau OA, Choi JY (2002) An energy decaying scheme for nonlinear dynamics of shells. Comput. Methods Appl. Mech. Engrg 1921: 3099–3121
7. Chung J, Hulbert G (1993) A time integration algorithm for structural dynamics with improved numerical dissipation: the generalized α method. ASME J. Appl. Mech. 60: 371–375
8. Crisfield MA, Galvanetto U, Jelenić G (1997) Dynamics of 3-D co-rotational beams. Comput. Mech. 20: 507–519
9. Erlicher S, Bonaventura L, Bursi OS (2002) The analysis of the Generalized -α method for the non-linear dynamic problems. Comput. Mech. 28: 83–104
10. Fung TC (2003) Numerical dissipation in time-step integration algorithms for structural dynamic analysis. Prog. Struct. Engrg. Mater. 5: 167–180
11. Gams M, Planinc I, Saje M (2006) Energy conserving integration scheme for geometrically exact beams. Comput. Methods Appl. Mech. Engrg. (Submitted for publication)
12. Gams M, Srpčič S, Saje M, Planinc I (2006) Finite element dynamic analysis of geometrically exact beams. Comp. Struct. (Accepted for publication)
13. Hilber HM, Hughes TJR, Taylor RL (1977) Improved numerical dissipation for time integration algorithms in structural dynamics. Earthquake Eng. Struct. Dyn. 5: 282–292
14. Ibrahimbegović A, Mamouri S (1999) Nonlinear dynamics of flexible beams in planar motion: formulation and time-stepping scheme for stiff problems. Comp. Struct. 70: 1–22
15. Ibrahimbegović A, Mamouri S (2002) Energy conserving/decaying implicit time-stepping scheme for three-dimensional beams undergoing finite rotations. Comput. Methods Appl. Mech. Engrg. 191: 4241–4258
16. Ibrahimbegović A, Mamouri S, Taylor RL, Chen AJ (2000) Finite element method in dynamics of flexible multibody systems: Modeling of holonomic constraints and energy conserving integration schemes. Multibody Sys. Dyn. 4: 195–223
17. Korelc J (1997) Automatic generation of finite-element code by simultaneous optimization of expressions. Theor. Comput. Sci. 187: 231–248
18. Kuhl D, Crisfield MA (1999) Energy-conserving and decaying algorithms in non-linear structural dynamics. Int. J. Numer. Meth. Engrg. 45: 569–599
19. Kuhl D, Ramm E (1996) Constraint energy momentum algorithm and its application to non-linear dynamics of shells. Comput. Methods Appl. Mech. Engrg. 136: 293–315
20. MATLAB (1999) Using MATLAB, the language of technical computing, The MathWorks, Inc., Natick, MA
21. Newmark NM (1959) A method of computation for structural dynamics. J. Eng. Mech. Div. ASCE 85: 67–94
22. Reissner E (1972) On one-dimensional finite-strain beam theory: the plane problem. J. Appl. Math. Physics (ZAMP) 23: 795–804
23. Sansour C, Wriggers P, Sansour J (1997) Nonlinear dynamics of shells: Theory, finite element formulation and integration schemes. Nonlinear Dyn. 13: 279–305
24. Sansour C, Wagner W, Wriggers P, Sansour J (2002) An energy-momentum integration scheme and enhanced strain finite elements fot he non-linear dynamics of shells. Int. J Non-Lin. Mech. 37: 951–966
25. Sansour C, Wriggers P, Sansour J (2003) A finite element post-processed Galerkin method for dimensional reduc-

tion in the non-linear dynamics of solids. Application to shells. Comput. Mech 32: 104–114

26. Sansour C, Wriggers P, Sansour J (2004) On the design of energy-momentum integration schemes for arbitrary continuum formulations. Applications to classical and chaotic motion of shells. Int. J. Numer. Meth. Engrg. 60: 2419–2440
27. Simo JC, Vu-Quoc L (1986) On the dynamics of flexible beams under large overall motions – The plane case: Part I and Part II. ASME J. Appl. Mech. 53: 849–854
28. Simo JC, Tarnow N, Doblare M (1995) Non-linear dynamics of three-dimensional rods: exact energy and momentum conserving algorithms. Int. J. Numer. Methods Engrg. 38: 1431–1473

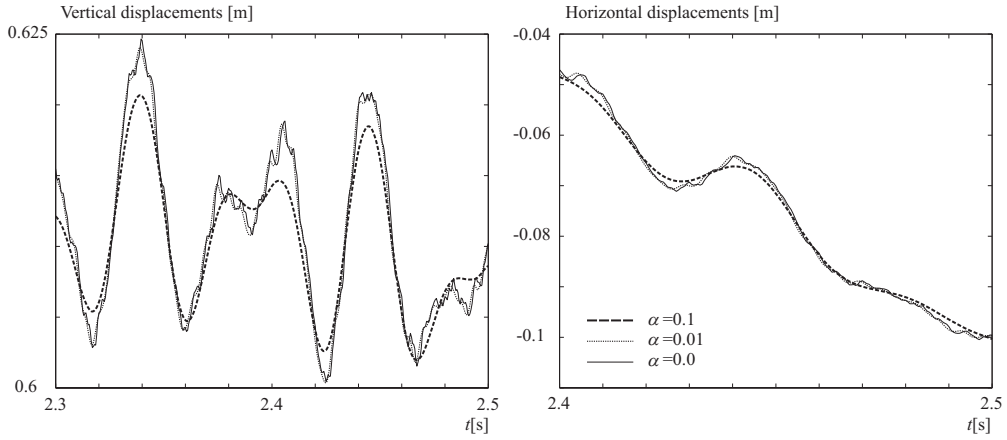

Fig. 5 Swinging pendulum. Magnification of the displacements. $\beta = 100$, $\tilde{\gamma} = \tilde{\delta} = 5$ in cases with damping.

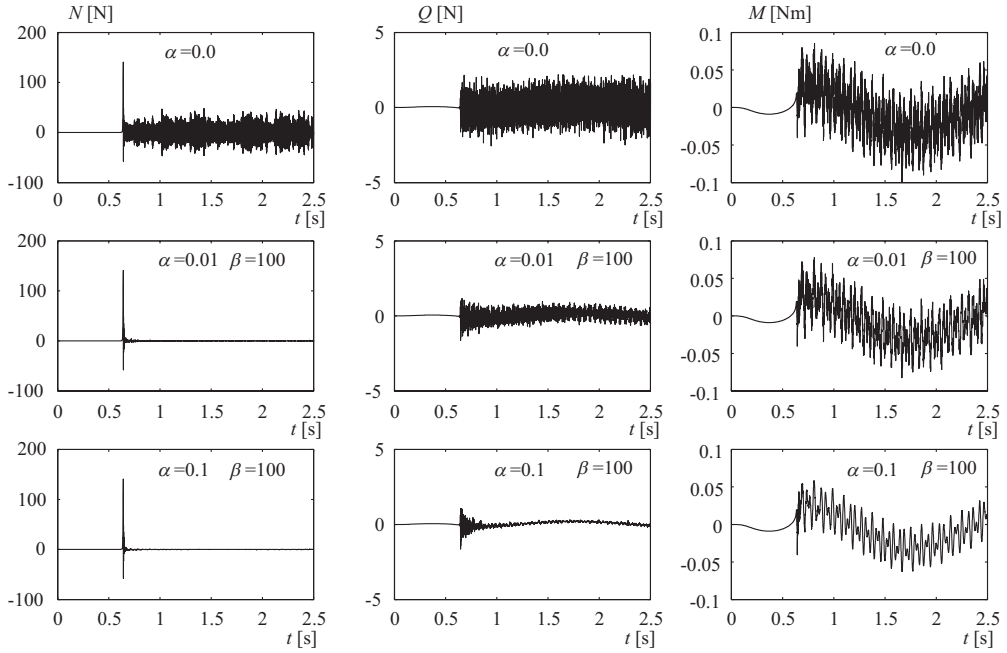

Fig. 8 Swinging pendulum. Internal forces at Gauss point immediately to the left of point B.

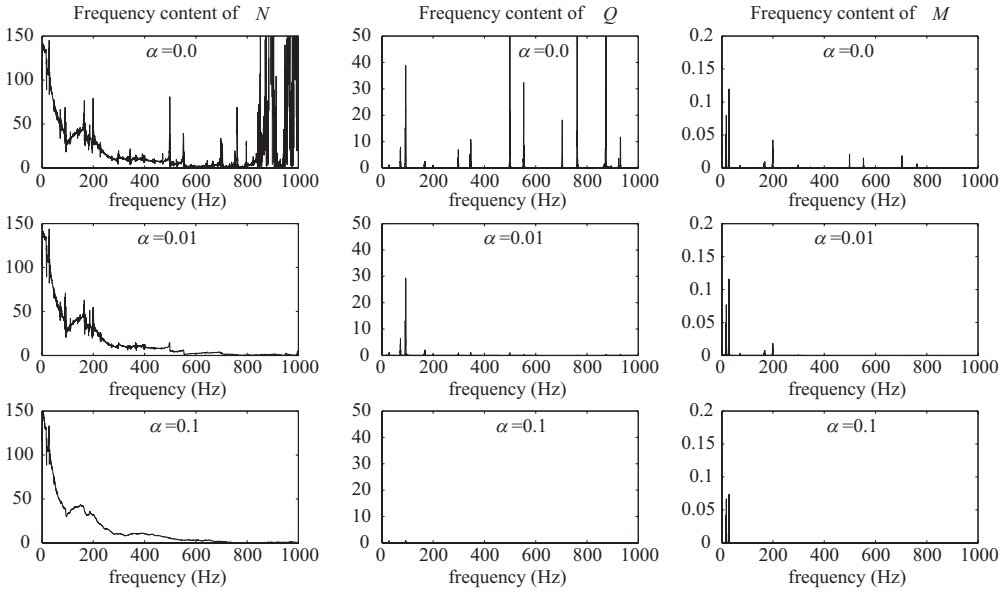

Fig. 9 Swinging pendulum. Frequency spectrum of internal forces at Gauss point immediately to the left of point B. $\beta = 100, \tilde{\gamma} = \tilde{\delta} = 5$.

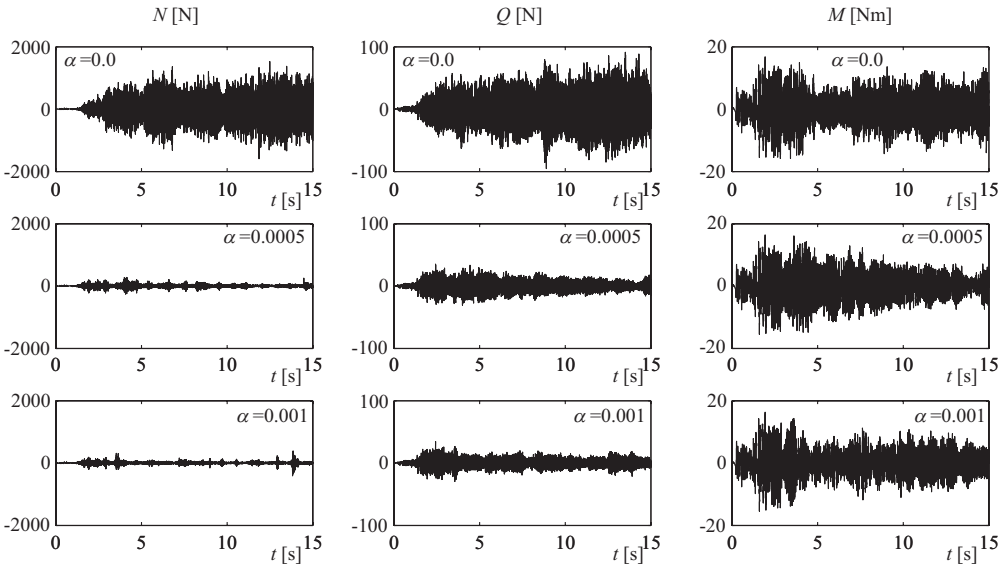

Fig. 13 Multibody system. Internal forces at Gauss point immediately to the left of point B. $\tilde{\gamma} = \tilde{\delta} = 5$ in cases with damping.

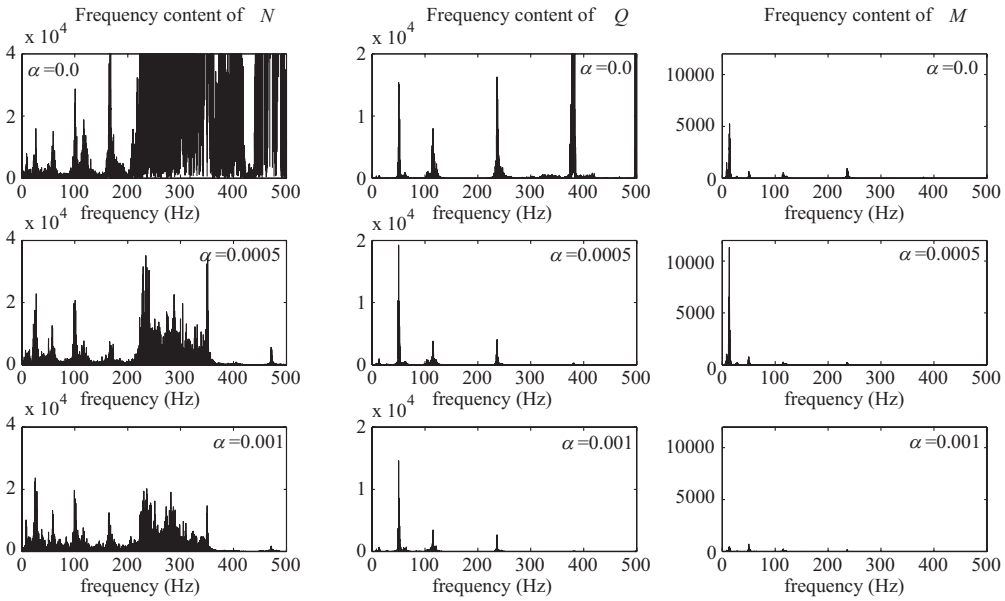

Fig. 14 Multibody system. Frequency spectrum of internal forces at Gauss point immediately to the left of point B. $\beta = 10, \tilde{\gamma} = \tilde{\delta} = 5$.

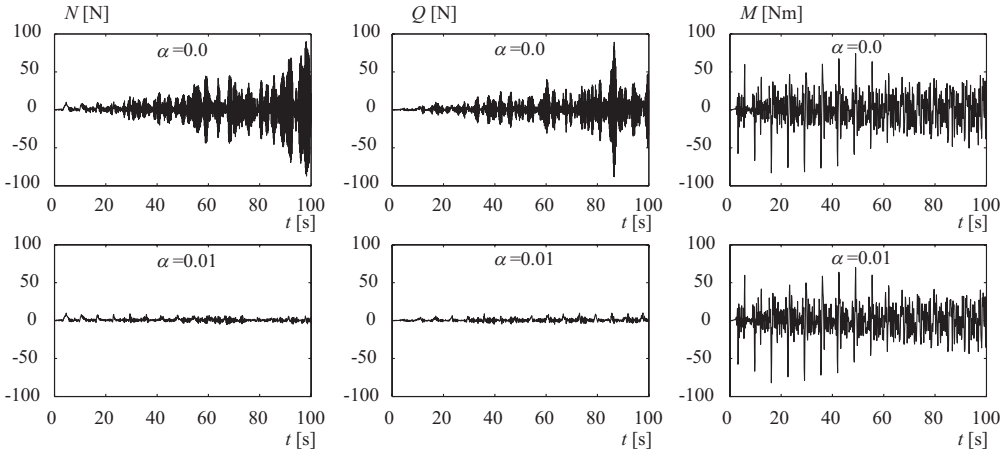

Fig. 18 Flying spaghetti. Internal forces at the first Gauss point to the right of point B. $\tilde{\gamma} = \tilde{\delta} = 5$.